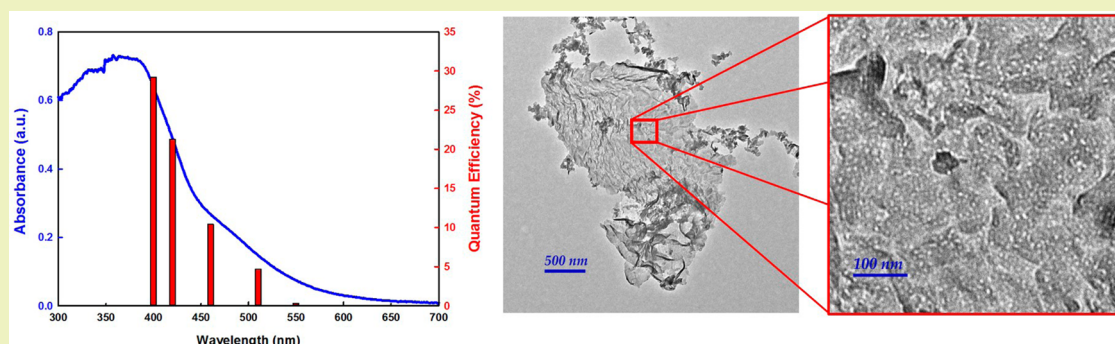# Post-Calcined Carbon Nitride Nanosheets as an Efficient Photocatalyst for Hydrogen Production under Visible Light Irradiation

Mohammad Reza Gholipour,[†] Francois Béland,[‡] and Trong-On Do[*,†]

[†]Department of Chemical Engineering, Laval University, Québec City, Québec G1V 0A8, Canada
[‡]SiliCycle Inc., 2500, Boul. du Parc-Technologique, Québec City, Québec G1P 4S6, Canada

ABSTRACT: Hydrogen production via photocatalytic water splitting using sunlight has enormous potential to solve the worldwide energy and environmental crisis. The key challenge in this process is to develop efficient photocatalysts which must satisfy several criteria such as strong sunlight absorption, effective charge separation, and high photochemical stability. Graphitic carbon nitride is one of the best semiconductors for hydrogen evolution because of its conduction band edge, narrow band gap, and high chemical stability. However, it produces a small amount of hydrogen under visible light irradiation due to its small surface area and high recombination rates. In this work, nanosheets of graphitic carbon nitride with carbon vacancies and nanoholes were synthesized by a two-step treatment process (argon treatment followed by air calcination). These post-calcined carbon nitride nanosheets exhibited much higher photocatalytic activity compared to common graphitic carbon nitride. By depositing platinum as a cocatalyst via a photodeposition method, this semiconductor showed noticeable improvement in hydrogen production rate at 10 times that of graphitic carbon nitride. Its hydrogen evolution rate was 5261 μmol h^{-1} g^{-1} under visible light illumination with a quantum efficiency of 29.2% at 400 nm and 21.3% at 420 nm. This high amount of hydrogen production rate could be due to large specific surface area, an extension of visible light absorption tail-end, and lower charge recombination centers throughout the semiconductor. In addition, by a recalcination step in air, some defects are introduced into the structure of carbon nitride nanosheets owing to carbon vacancies. These defects are considered to be highly active photocatalytic sites for hydrogen production.

KEYWORDS: Photocatalyst hydrogen production, Visible light photocatalyst, Graphitic carbon nitride, High quantum efficiency photocatalyst

INTRODUCTION

Development of technology requires a cheap and accessible source of energy. Although fossil fuels are the most well-known sources of energy for their low cost and availability, they have some important issues for humans such as emission of a high amount of carbon dioxide into the atmosphere which is believed to be the main reason for the greenhouse effect and climate change. Others claim that fossil fuel resources are limited and cannot be recovered once they are used. Therefore, researchers have tried to find other alternatives for fossil fuels, and the best option is solar energy.

Solar energy is abundant, and only a very small amount of it can provide all the energy demands of humanity around the world for one year.[1,2] Moreover, this source of energy is

renewable and sustainable, which means there is no way to overconsume it in the present or future. Interestingly, sunlight energy is environmentally friendly, and it does not produce any harmful gases; as a result, we will not have any climate crisis in the future.[2] However, using this source of energy is quite expensive, and so it is very difficult to utilize it in large scale applications.

Hydrogen molecules can act as an energy carrier in order to store solar energy and use it later. One of the most promising ways to produce hydrogen energy is to split water into

hydrogen and oxygen with the photocatalytic process. A photocatalyst is a semiconductor that can absorb sunlight energy and generate excited electrons and holes. These charge carriers can perform redox reactions with water molecules and so generate hydrogen and oxygen.[3] One of the best photocatalysts for using solar energy is graphitic carbon nitride (g-C$_3$N$_4$), because of its low band gap energy that can utilize visible light to produce hydrogen from water.[4,5]

Graphitic carbon nitride (g-C$_3$N$_4$) is a semiconductor consisting of tri-s-triazine units positioned in a two-dimensional graphitic-like polymer structure.[6] Due to its proper conduction band-edge position and narrow band gap, which is between 2.7 and 2.9 eV corresponding to wavelengths 460−430 nm, it can generate hydrogen from water splitting under visible light irradiation.[7,8] However, its quantum efficiency is very low mainly due to its small specific surface area and rapid charge recombination rate.[9,10] The main synthesis method of g-C$_3$N$_4$ is a thermal condensation (at 500−550 °C for 2−4 h) of nitrogen-rich precursors such as cyanamide, dicyandiamide, urea, and melamine.[1,8,11] Thermogravimetric analysis (TGA) shows that g-C$_3$N$_4$ is stable up to 600 °C even in the air, but becomes slightly unstable above this temperature, and at 700 °C, it completely disappears even under an inert gas condition.[7,12,13]

Various methods and techniques were proposed in order to enhance the photocatalytic activity of g-C$_3$N$_4$, and they can be classified into four main groups as electronic structure modulation, nanostructure design, crystal structure engineering, and heterostructure construction.[8,9] Some of these such as synthesizing nanosheets of g-C$_3$N$_4$ can enhance hydrogen evolution significantly due to high specific surface area, enhanced charge carrier mobility, and fewer charge recombination centers.[14−17] In this work, a facile two-step synthesis method for the synthesis of g-C$_3$N$_4$ nanosheets with some carbon vacancies and micropores is proposed that can considerably increase hydrogen production under visible light illumination. This photocatalyst showed a quantum efficiency of 29.20% at 400 nm, which is among the highest quantum efficiencies that have been previously reported.

■ EXPERIMENTAL SECTION

Sample Preparation. Bulk g-C$_3$N$_4$ was synthesized from dicyandiamide as reported in other literature studies.[18−20] Briefly, the precursors were calcined in a muffle furnace at 550 °C in air for 4 h. Then, the obtained bulk g-C$_3$N$_4$ (GCN) was washed with distilled water several times. After this step, the photocatalyst was heated to 650 °C under an argon gas flow of 200 mL/min for 2 h (argon treatment of g-C$_3$N$_4$, noted as AGCN). After this stage is completed, the obtained material was calcined again in the air, in a muffle furnace at 500 °C for 2 h (recalcination of AGCN of g-C$_3$N$_4$ in air, noted as SGCN). Then, the material was washed several times with water to remove contaminants and dried in an oven overnight at 70 °C.

Characterization. Transmission electron microscopy (TEM) images of the samples were obtained on a JEOL JEM 1230 operated at 120 kV. Powder X-ray diffraction (XRD) patterns of the samples were obtained on a Bruker SMART APEXII X-ray diffractometer equipped with a Cu Kα radiation source (λ = 1.5418 Å). X-ray photoelectron spectroscopy (XPS) measurements carried out in an ion-pumped chamber (evacuated to 10^{-9} Torr) of a photoelectron spectrometer (Kratos Axis-Ultra) equipped with a focused X-ray source (Al Kα, hν = 1486.6 eV). The UV−vis spectra were recorded on a Cary 300 Bio UV−vis spectrophotometer. Fourier transform infrared (FTIR) absorption spectra were measured with an FTS 45 infrared spectrophotometer with the KBr pellet technique. The photoluminescence (PL) spectra were measured with the Horiba Jobin

Yvon Nanolog spectrofluorimeter equipped with a 450 W xenon lamp as a source, a double monochromator for both excitation and detection, and a photomultiplier tube (PMT) detector sensitive from 250 to 850 nm. Nitrogen adsorption−desorption isotherms of the samples were measured at −196 °C using Micromeretics ASAP 2010 instrument. Before the measurements, the samples were outgassed under vacuum for 6 h at 150 °C. The total pore volume (V_{pore}) was calculated from the amount of nitrogen adsorbed at $P/P_0 = 0.95$.

Photocatalytic Test. The certain amount of photocatalysts (the optimum amount was 50 mg) was added to the 100 mL of aqueous solution of 10% triethanolamine as a sacrificial reagent. After that, the mixture was purged with nitrogen for 10 min, and then under the solar simulator light, 2 wt % Pt as the cocatalyst was deposited via photodeposition technique for 2 h. Then, the cell was purged again with nitrogen for 30 min, and after this the sample was ready for a hydrogen production test over 3-h cycles.

The quantum efficiency of the prepared sample was calculated according to follow equations:[21,22]

$$
\begin{aligned}
\text{quantum efficiency (QE)} \\
= \frac{\text{number of reacted electrons}}{\text{number of incident photons}} \times 100 \\
= \frac{2 \times \text{number of evolved hydrogen molecules}}{\text{number of incident photons}}
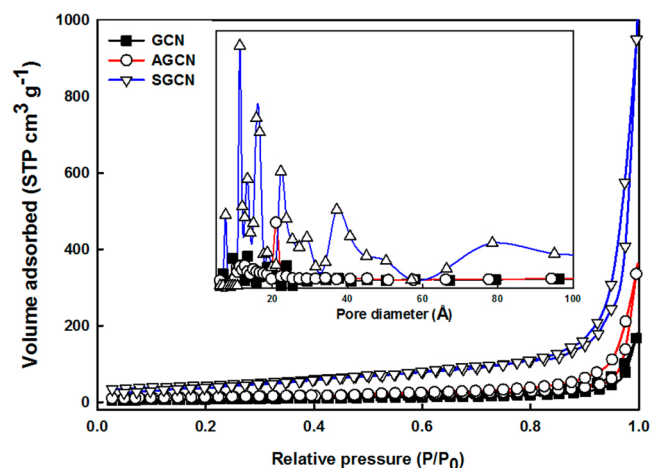\end{aligned}
\tag{1}
$$

■ RESULTS AND DISCUSSION

Material Characterization. Figure 1 demonstrates a 2D nanosheet of SGCN sample after recalcination in air in different scales. Although the nanosheet length and width are more than several hundred nanometers (Figure 1A,B), AFM analysis shows that the thickness of the nanosheet hardly reaches 10 nm (Figure 1G,H).[23−25] Furthermore, as can be seen in Figure 1E, there are some uniform small white dots all over the nanosheets that can be described as nanoholes and carbon vacancies generated during the second calcination step in air.[25] Due to the layered structure of graphitic carbon nitride, these vacancies were created homogeneously inside the nanosheet planes. These vacancies with a size of less than 10 nm not only can act as active sites but also can change the band gap of the photocatalyst by introducing additional energy levels.[26−28] It should be noted that these in-plane nanoholes can noticeably enhance mass and charge transfer across the nanosheets of SGCN during the photocatalytic process.[25,29] Moreover, ultrathin nanosheets provide shorter pathways for photoexcited charges to migrate significantly shorter distances from the bulk material to the reaction sites located on its surfaces.[1,30,31] In addition, carbon vacancies can act as new active edges and cross-plane diffusion channels that can greatly speed up mass transfer and the diffusion of photogenerated charge carriers.[25,29] Therefore, charge carriers can travel shorter distances between the inside of the nanosheets and their surfaces in order to reach the active sites, and so, the chance of their recombination reduced dramatically. Figure 1F displays a TEM image of SGCN with photodeposited platinum nanoparticles after photocatalysis reaction. It is obvious that the cocatalyst particles are uniformly deposited on the surface of nanosheets of SGCN.

Figure 2 displays the N$_2$ adsorption/desorption isotherms of three samples: GCN, AGCN, and SACN at 77 K. All of the samples showed a type IV isotherm, and their adsorption capacity enhanced significantly with increasing the relative pressure (P/P_0: 0.9−1). The specific surface area measured by the BET technique increased considerably and reached 160 m^2 g^{-1} for SGCN (Table 1). This specific surface area is much higher than those of AGCN and GCN, which were 46 and 28
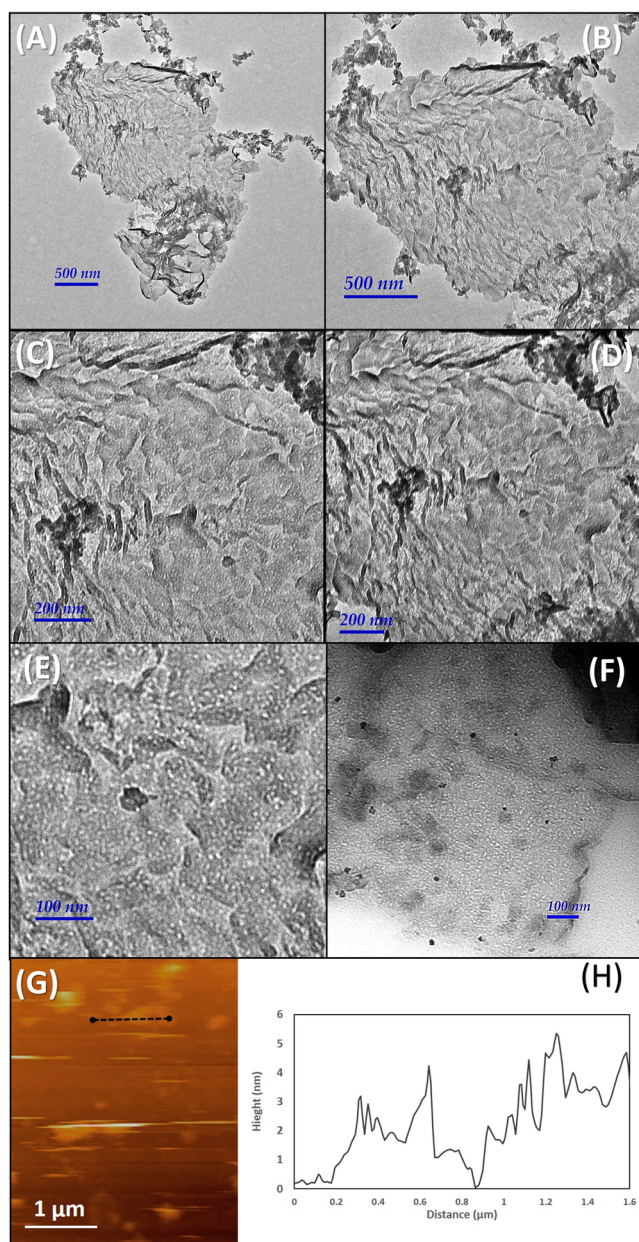
Figure 1. (A−E) TEM images of two-dimensional SGCN nanosheets after recalcination in air at different scales (small white dots show nanoholes inside of the nanosheet of SGCN). (F) Nanosheets of SGCN with 2% Pt after photodeposition. (G) Representative AFM image of SGCN and (H) corresponding cross-sectional profile of typical SGCN.

Figure 2. Nitrogen adsorption−desorption isotherms at 77 K and relating pore size distribution curves of GCN, AGCN, and SGCN (inset).
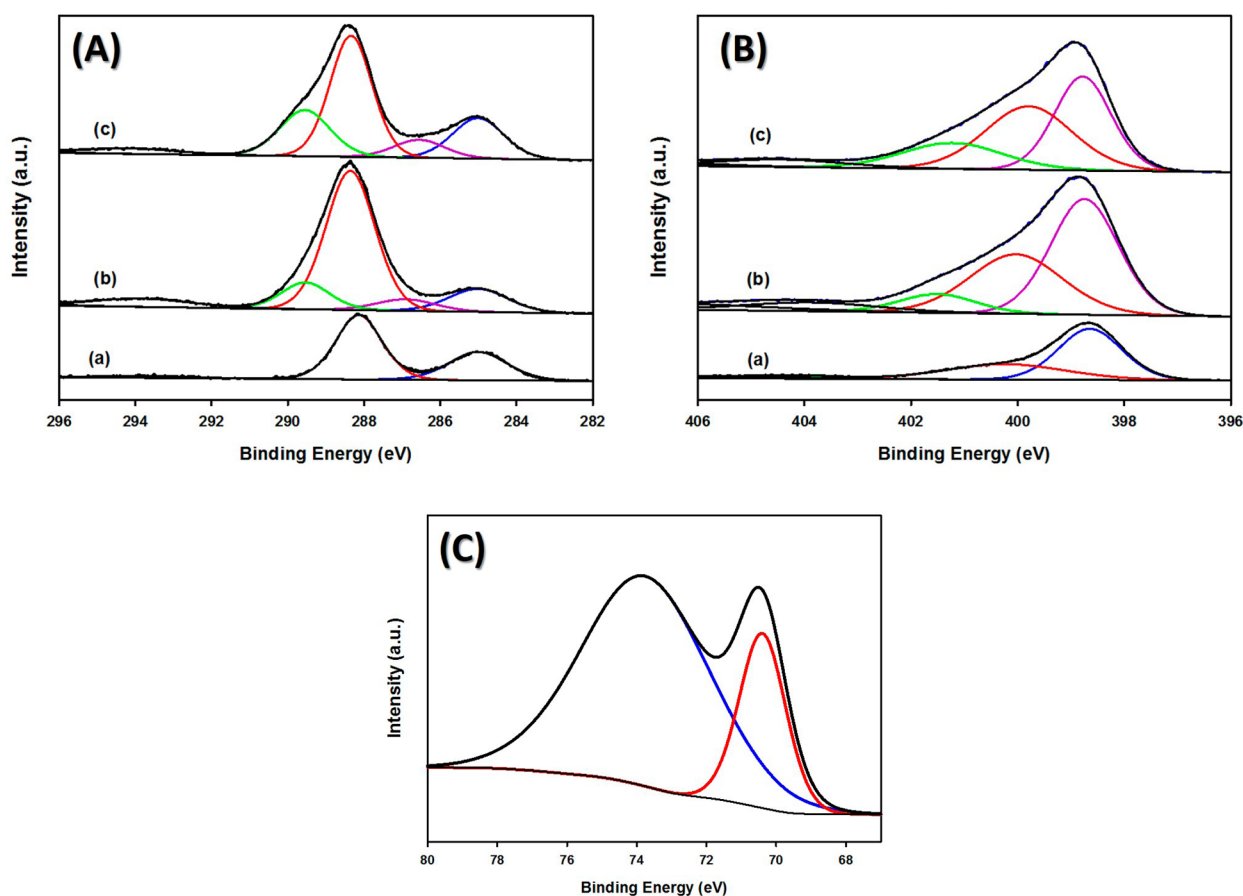
Table 1. Total Pore Volume, Specific Surface Area, Band Gap Values, and Hydrogen Generation Rate of GCN, AGCN, and SGCN

sample	total pore volume (cm^{-3} g^{-1})	BET surface area (m^2 g^{-1})	band gap (eV)	hydrogen production (μmol h^{-1} g^{-1})
GCN	0.12	28.0	2.75	647.5
AGCN	0.52	45.0	2.56	771.5
SGCN	1.47	160.0	2.79	5262.0

distances and carbon vacancies throughout the SGCN nanosheets that were made during the second calcination in air as described in TEM images (Figure 1).[25,29,32]

Figure 3 shows the XPS spectra of the bulk sample (GCN) after different treatments: argon treatment (AGCN), followed by calcination in air (SGCN). As seen in Figure 3, the C 1s and N 1s XPS spectra of GCN, AGCN, and SGCN are almost similar to each other. Nonetheless, an increase in the intensities of AGCN and SGCN illustrated that C and N atoms neighboring carbon vacancies get fewer electrons than those ones on the normal sites.[25] As seen in Figure 3A, the C 1s XPS spectrum of GCN can be deconvoluted into two main peaks at 285.0 and 288.1 eV, which are attributed to C—C and N—C═N, respectively.[8] Moreover, the C 1s XPS spectra of AGCN and SGCN can be resolved into two additional peaks. The peak observed at 289.6 eV can correspond to the sp^2 carbon of tri-s-triazine units attached to the NH group (sp^2 C—NH). The other peak at 286.5 eV is related to sp^3 C atoms in the structure of carbon nitride. Furthermore, the absorptions detected around 294 eV have been assigned to the charge effect of electronic delocalization associated with the presence of conjugation.[32]

In the N 1s XPS spectra (Figure 3B), the main curve can be divided into four peaks. The peaks located at 398.7 eV are related to the sp^2-bonded nitrogen in C—N═C, and the peaks corresponding to the nitrogen in the tertiary group (N—(C)$_3$) are located at 400.1 eV. Moreover, the amino-functional groups with a hydrogen atom C—NH can be attributed to 401.5 eV, and the absorption at 404.0 eV is due to a positive charge localization in heptazine rings.[32,33] According to these XPS analyses, during argon treatment at high temperature some carbon atoms in the structure of GCN became loose, and as a

m^2 g^{-1}, respectively. It should be noted that the total pore volume of SGCN (1.47 cm^3 g^{-1}) is around 13 times higher than that of GCN (0.12 cm^3 g^{-1}). This increase in specific surface area and total pore volume is due to a large number of in-plane holes and the crumpled structure. Furthermore, the BJH pore size distribution curves were also demonstrated in Figure 2, inset. Although it seems that the pore size distribution of GCN and AGCN argon-treated at 650 °C were almost similar, treatment in argon at high temperature led to having more uniform pore size distribution. Nevertheless, the SGCN showed a wide range of pore sizes between 1 and 5 nm that demonstrated the SGCN is the mixture of micropores and mesopores. These pores were mainly related to interparticle

Figure 3. High-resolution XPS survey spectra of (A) C 1s and (B) N 1s for (a) GCN, (b) AGCN, and (c) SGCN. (C) High-resolution XPS of the Pt 4f region for Pt-SGCN photodeposited after photocatalysis.

result, a few of them were able to leave the bulk material, leaving some carbon vacancies behind in the SGCN. Following by further calcination in air, more loose carbons were able to leave carbon nitride. As a result, not only did the number of carbon vacancies increase, but also some uniform nanoholes were produced.

In order to investigate the valence state of platinum as a cocatalyst, XPS analysis of Pt 4f after photocatalysis reaction was conducted. The main peak of Pt 4f can be deconvoluted into two peaks at 70.4 and 73.9 eV, which are ascribed to metallic Pt 4f7/2 and Pt 4f5/2, respectively.[34−36]

Figure 4 presents the X-ray diffraction (XRD) results of the synthesized bulk g-C$_3$N$_4$ material after different treatments. The crystal structure of bulk g-C$_3$N$_4$ (e.g., GCN) is shown by two main peaks of (100) and (002), which are located at 13.1° and 27.4°, respectively. The former peak is ascribed to the in-plane trigonal nitrogen linkage of tri-s-triazine units, and the latter one is related to the periodic stacking of layers of conjugated aromatic systems.[8] The disappearance of the 13.1° peak of AGCN shows that the long-range order of atomic arrangements in graphitic layers of AGCN is destroyed, and as a result, AGCN can be considered as an amorphous phase of carbon nitride.[23,25,32,37] In addition, the other peak with very low intensity at 27.4° indicates that we have g-C$_3$N$_4$ nanosheets, as displayed in TEM images. In other words, the distance between different layers of g-C$_3$N$_4$ increased significantly, and so nanosheets of g-C$_3$N$_4$ were obtained.[24,33]

After recalcination in air (e.g., SGCN sample), the crystal structure of carbon nitride nanosheets improves moderately,
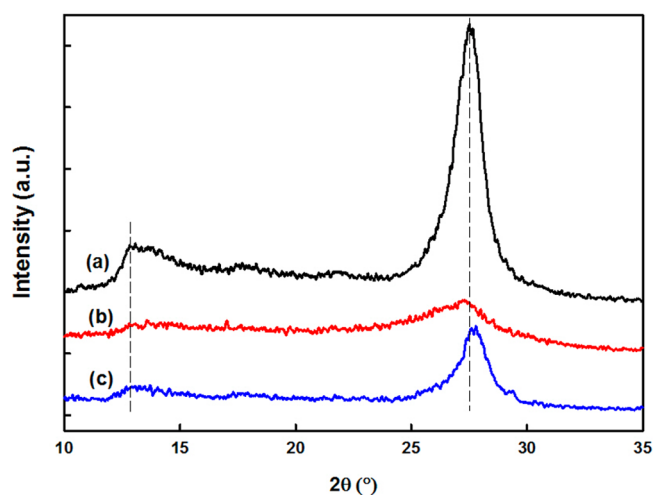
Figure 4. X-ray diffraction analyses of (a) GCN, (b) AGCN, and (c) SGCN.

and as a result, the two peaks appeared again. However, because of obtaining nanosheets and some vacancies inside of the planes of graphitic carbon nitride, the restructuring could not be completed, and so the intensity of the (002) peak was not as high as that of GCN. It is worth mentioning that, during recalcination, most of the weakly bonded carbon and nitrogen atoms left from the bulk material in forms of various gases. These generated gases acted as a soft template in order to produce ultrathin nanosheets of graphitic carbon nitride.[15] In

216

addition, this leaving of weakly bonded atoms generated many more vacancies and nanoholes throughout the nanosheets, which improved hydrogen generation in various ways as mentioned earlier.[19,38]

Figure 5 illustrates the FTIR spectra of the GCN, AGCN, and SGCN samples to investigate their graphitic structures.
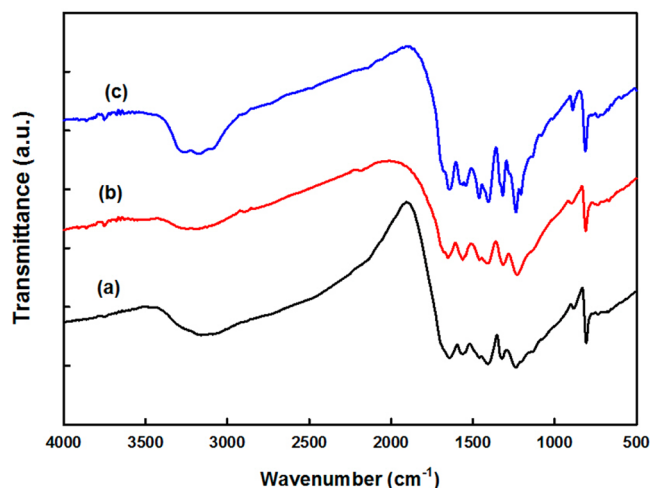

Figure 5. FTIR spectra of (a) GCN, (b) AGCN, and (c) SGCN.

The strong peak at 810 cm^{-1} is attributed to the typical breathing mode of tri-s-triazine units.[39] The absorption bands in the 1200−1700 cm^{-1} region are related to different stretching vibrations of heptazine-derived repeating units.[40,41] In addition, broad peaks from 3000 to 3400 cm^{-1} corresponded to the N−H band, which is caused by uncondensed amino-functional groups in the products.[42] There is no difference between FTIR spectra of the three materials suggesting that the nature of carbon nitride was preserved during argon treatment and recalcination in air.

UV−vis spectroscopy is usually used in order to measure the light absorption capacity of the semiconductors, and also, its data can be used to calculate band structure and band gap of a photocatalyst. UV−vis spectra of GCN, AGCN, and SGCN were presented in Figure 6. GCN can absorb visible light with a wavelength of 420 nm, because of its low band gap (2.75 eV). After argon treatment at 650 °C, the UV−vis spectrum of AGCN shifted to the red region, and its band gap reduced to

2.56 eV (Figure 6B). Even though it could absorb visible light with a longer wavelength, it could not produce more hydrogen than GCN. This is due to its low crystallinity (essentially amorphous phase) and a high number of recombination centers. In addition, the band structure of AGCN seemed to not develop completely because of observing two stages in its UV−vis spectrum (the curve is different below and above 450 nm). Nonetheless, the SGCN spectrum showed that, by recalcination in air, its curve shifted to the blue region, and so the band gap increased (to 2.79 eV). Moreover, this recalcination step helped to improve crystal structure, and as a result, more charge carriers can transfer more easily across the nanosheets which limit recombination together. In addition, another absorption tail started at 430 nm to around 600 nm and exhibited that the SGCN can absorb more visible light energy in comparison with GCN. It is worth mentioning that the crystallinity changes between amorphous and graphitic layer structure of nanosheets may introduce some different band energy inside the band gap structure as shown by Chen et al.[43] These intermediate band energies can promote charge excitation as well as charge lifetime. In other words, not only does the charge excitation step become easier, but also photoexcited charge carriers have different stages which could help them to have less recombination process.

Figure 7 displays the steady-state photoluminescence spectra of all three samples. The prepared bulk GCN showed the highest peak intensity with respect to AGCN and SGCN relating to the high radiative recombination of photoexcited electrons and holes.[23,43,44] In contrast, SGCN exhibited the lowest peak intensity, suggesting a much lower charge recombination process during photocatalytic activity.

Photocatalytic Hydrogen Production. Figure 8A demonstrated the hydrogen production of the three samples, GCN, AGCN, and SGCN, via solar simulator system with full spectrum. As seen in Figure 7A, AGCN could only slightly improve hydrogen generation compared to that of GNC. However, SGCN could enhance hydrogen evolution more than eight times higher than GCN (5261 μmol h^{-1} g^{-1} for SGCN and 647 μmol h^{-1} g^{-1} for GCN). This considerable increase in hydrogen generation is mainly due to the presence of carbon vacancies, the high surface area, and the extension tail of light absorption. The carbon vacancies not only can act like a trapping spot for excited charge carriers, but also can promote mass transfer between nanosheets that help to have a higher
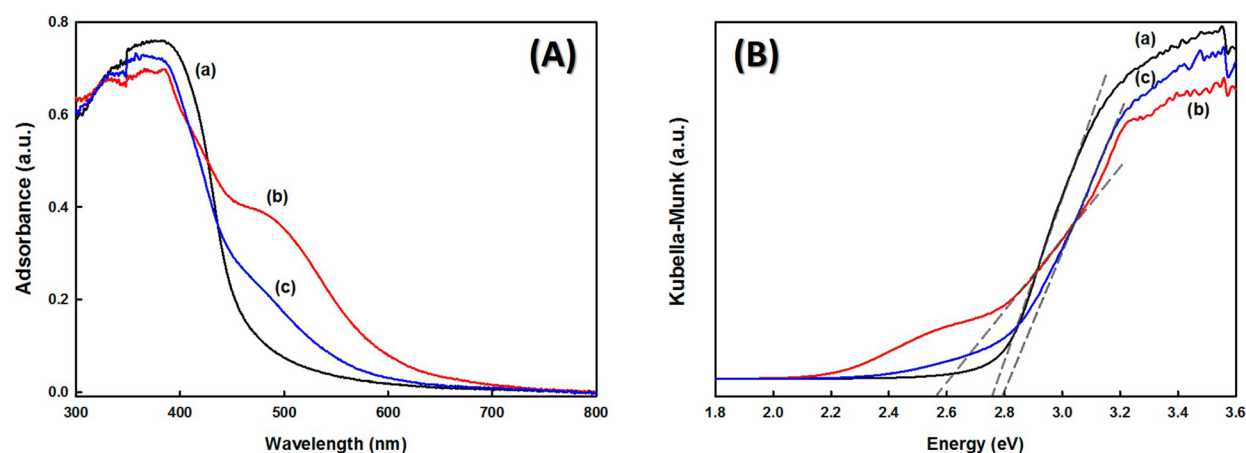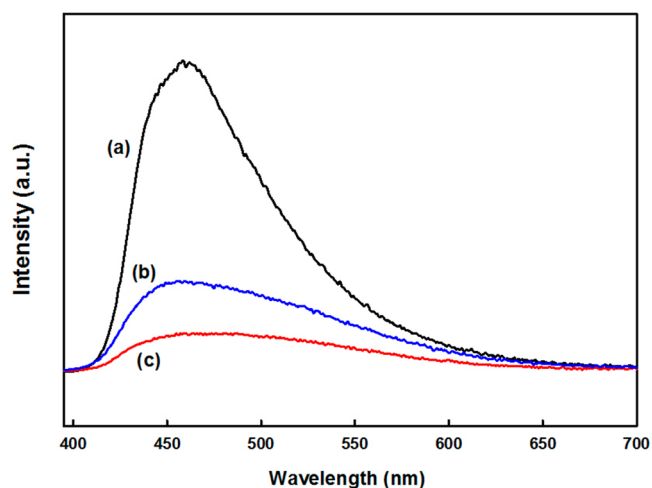

Figure 6. (A) UV−visible absorption spectra and (B) Kubelka−Munk function curves of (a) GCN, (b) AGCN, and (c) SGCN.

Figure 7. Photoluminescence spectra (390 nm excitation) of (a) GCN, (b) AGCN, and (c) SGCN (steady-state emission spectra were recorded on a powdered sample under excitation wavelength of 380 nm).

hydrogen generation. Furthermore, these nanoholes inside of SGCN nanosheets could act as active sites for reactants.

Moreover, the improvement in the structure of SGCN after the second calcination, as shown in Figure 4, enhances the charge mobility inside the nanosheet of graphitic carbon nitride.

For further investigation, hydrogen generation under visible light with the same system was studied with applying a light filter that surpasses wavelengths of lower than 420 nm (Figure 8B). Due to a decrease in the band gap of AGCN and the fact that it can absorb more visible light, it could produce more hydrogen than GCN under visible light irradiation. The hydrogen evolution rates were 104 and 85 μmol h^{-1} g^{-1} for AGCN and GCN, respectively. However, SGCN showed significantly higher hydrogen production in the same conditions in comparison with the other two samples. Interestingly, it generated 387 μmol h^{-1} g^{-1} hydrogen, which was about 4.5 times higher than that of GCN.

Furthermore, the quantum efficiency of SGCN was also calculated with different band-pass filters (band-pass filters at 400, 420, 460, 500, and 550 nm). As exhibited in Figure 8C, the highest quantum efficiency was 29.2% which was obtained at 400 nm. This amount is among the highest quantum efficiency which was reported for graphitic carbon nitride under visible light illumination. In addition, the quantum efficiency calculated at 420 nm was 21.3% that shows very high hydrogen evolution in the visible light region. Because of the large band
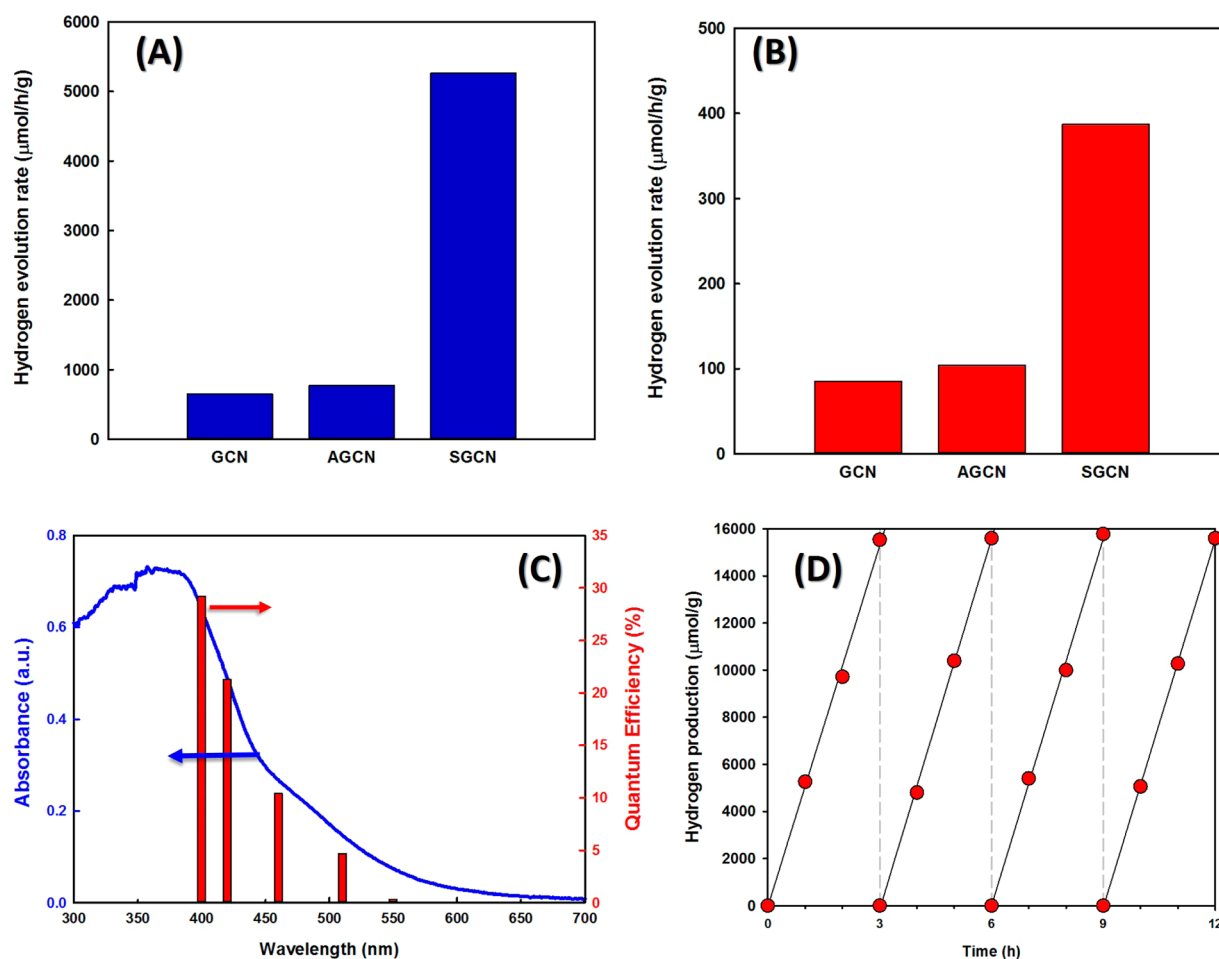
Figure 8. (A) Hydrogen evolution rate under full spectrum via solar simulator system. (B) Hydrogen generation rate under visible light irradiation with a solar simulator (λ > 420 nm). (C) UV−vis spectrum and quantum efficiency of the SGCN sample. (D) Hydrogen production of the SGCN for 4 cycles. Reaction conditions: 50 mg of photocatalyst loaded with 2 wt % of Pt cocatalyst; 100 mL of H$_2$O containing 10 vol % triethanolamine under simulator solar light 1.5 AM (ABET), equipped with 150 W Xe lamp.

gap of SGCN nanosheets, the quantum efficiency decreased for longer light wavelengths and reached almost 0.34% for 550 nm (Figure 8C). Furthermore, the SGCN generated hydrogen over 12 h without any reduction in its activity for hydrogen production (Figure 8D). It is worth mentioning that the SGCN has a great potential to combine with other semiconductors (nanocomposite systems) and metals (as cocatalysts), because of its special properties such as large surface area and enormous active sites all over the nanosheets of SGCN.

CONCLUSION

Photocatalytic hydrogen evolution from sunlight energy is one of the best options for fossil fuel replacement. Graphitic carbon nitride is one of the best photocatalysts for hydrogen production under the visible light because of its low band gap that can absorb the energy of light in the visible region. By synthesizing post-calcined nanosheets of graphitic carbon nitride with facile two-step calcination (argon treatment followed by air recalcination), ultrathin nanosheets of carbon nitride with carbon vacancies and nanoholes were obtained. This photocatalyst showed considerably higher specific surface area (160 m^2/g) and better crystallinity compared to the amorphous phase of carbon nitride. Existence of nanoholes and carbon vacancies throughout the nanosheets caused more active sites for reactants as well as more charge trapping centers that can reduce the charge recombination process. By applying platinum as a cocatalyst, this new photocatalyst could generate hydrogen at a rate of 5261 μmol h^{-1} g^{-1} under sunlight irradiation. Moreover, the hydrogen evolution rate under visible light ($\lambda \geq$ 420 nm) was around 387 μmol h^{-1} g^{-1}. In order to compare this novel photocatalyst with graphitic carbon nitride, the quantum efficiency (QE) of the band-pass filter was calculated. The QE at 400 nm was 29.2%, and at 420 nm it was 21.3%. These values are among the highest quantum efficiencies that were reported for graphitic carbon nitride under visible light illumination.

AUTHOR INFORMATION

Corresponding Author
*E-mail: Trong-On.Do@gch.ulaval.ca. Phone: +1 (418) 656-3774.
ORCID
Trong-On Do: 0000-0002-7785-5299
Notes
The authors declare no competing financial interest.

ABBREVIATIONS

GCN: graphitic carbon nitride
AGCN: amorphous phase of graphitic carbon nitride, after argon treatment
SGCN: post-calcined graphitic carbon nitride, post-calcination in air after argon treatment

REFERENCES

(1) Gholipour, M. R.; Dinh, C.-T.; Béland, F.; Do, T.-O. Nanocomposite heterojunctions as sunlight-driven photocatalysts for hydrogen production from water splitting. *Nanoscale* 2015, 7 (18), 8187−8208.
(2) Lewis, N. S.; Crabtree, G.; Nozik, A. J.; Wasielewski, M. R.; Alivisatos, P. Basic Research Needs for Solar Energy Utilization. *Basic Energy Sci. Work. Sol. Energy Util.* 2005, 276.
(3) Li, X.; Yu, J.; Low, J.; Fang, Y.; Xiao, J.; Chen, X. Engineering heterogeneous semiconductors for solar water splitting. *J. Mater. Chem. A* 2015, 3 (6), 2485−2534.
(4) Dong, G.; Zhang, Y.; Pan, Q.; Qiu, J. A fantastic graphitic carbon nitride (g-C$_3$N$_4$) material: Electronic structure, photocatalytic and photoelectronic properties. *J. Photochem. Photobiol., C* 2014, 20, 33−50.
(5) Yin, S.; Han, J.; Zhou, T.; Xu, R. Recent progress in g-C$_3$N$_4$ based low cost photocatalytic system: activity enhancement and emerging applications. *Catal. Sci. Technol.* 2015, 5 (12), 5048−5061.
(6) Thomas, A.; Fischer, A.; Goettmann, F.; Antonietti, M.; Müller, J.-O.; Schlögl, R.; Carlsson, J. M. Graphitic carbon nitride materials: variation of structure and morphology and their use as metal-free catalysts. *J. Mater. Chem.* 2008, 18 (41), 4893.
(7) Wang, X.; Blechert, S.; Antonietti, M. *ACS Catal.* 2012, 2, 1596−1606.
(8) Cao, S.; Low, J.; Yu, J.; Jaroniec, M. Polymeric Photocatalysts Based on Graphitic Carbon Nitride. *Adv. Mater.* 2015, 27 (13), 2150−2176.
(9) Zheng, Y.; Lin, L.; Wang, B.; Wang, X. Graphitic Carbon Nitride Polymers toward Sustainable Photoredox Catalysis. *Angew. Chem., Int. Ed.* 2015, 54 (44), 12868−12884.
(10) Wang, X.; Maeda, K.; Thomas, A.; Takanabe, K.; Xin, G.; Carlsson, J. M.; Domen, K.; Antonietti, M. A metal-free polymeric photocatalyst for hydrogen production from water under visible light. *Nat. Mater.* 2009, 8 (1), 76−80.
(11) Zhang, J.; Chen, Y.; Wang, X. Two-dimensional covalent carbon nitride nanosheets: synthesis, functionalization, and applications. *Energy Environ. Sci.* 2015, 8 (11), 3092−3108.
(12) Khabashesku, V. N.; Zimmerman, J. L.; Margrave, J. L. Powder synthesis and characterization of amorphous carbon nitride. *Chem. Mater.* 2000, 12 (11), 3264−3270.
(13) Seredych, M.; Los, S.; Giannakoudakis, D. A.; Rodríguez-Castellon, E.; Bandosz, T. J. Photoactivity of g-C$_3$N$_4$/S-Doped Porous Carbon Composite: Synergistic Effect of Composite Formation. *ChemSusChem* 2016, 9, 795−799.
(14) Lin, Q.; Li, L.; Liang, S.; Liu, M.; Bi, J.; Wu, L. Efficient synthesis of monolayer carbon nitride 2D nanosheet with tunable concentration and enhanced visible-light photocatalytic activities. *Appl. Catal., B* 2015, 163, 135−142.
(15) Lu, X.; Xu, K.; Chen, P.; Jia, K.; Liu, S.; Wu, C. Facile one step method realizing scalable production of g-C$_3$N$_4$ nanosheets and study of their photocatalytic H$_2$ evolution activity. *J. Mater. Chem. A* 2014, 2 (44), 18924−18928.
(16) Martin, D. J.; Qiu, K.; Shevlin, S. A.; Handoko, A. D.; Chen, X.; Guo, Z.; Tang, J. Highly efficient photocatalytic H$_2$ evolution from water using visible light and structure-controlled graphitic carbon nitride. *Angew. Chem., Int. Ed.* 2014, 53 (35), 9240−9245.
(17) Wang, Y.; Hong, J.; Zhang, W.; Xu, R. Carbon nitride nanosheets for photocatalytic hydrogen evolution: remarkably enhanced activity by dye sensitization. *Catal. Sci. Technol.* 2013, 3 (7), 1703−1711.
(18) Zhang, G.; Lan, Z.-A.; Lin, L.; Lin, S.; Wang, X. Overall Water Splitting by Pt/g-C$_3$N$_4$ Photocatalysts without Using Sacrificial Agent. *Chem. Sci.* 2016, 7, 3062−3066.
(19) Niu, P.; Liu, G.; Cheng, H.-M. N Vacancy Nitrogen Vacancy-Promoted Photocatalytic Activity of Graphitic Carbon Nitride. *J. Phys. Chem. C* 2012, 116 (20), 11013−11018.
(20) Niu, P.; Zhang, L.; Liu, G.; Cheng, H.-M. Graphene-Like Carbon Nitride Nanosheets for Improved Photocatalytic Activities. *Adv. Funct. Mater.* 2012, 22 (22), 4763−4770.

(21) Chen, X.; Shen, S.; Guo, L.; Mao, S. S. Semiconductor-based photocatalytic hydrogen generation. *Chem. Rev.* **2010**, *110* (11), 6503−6570.

(22) Shimura, K.; Yoshida, H. Heterogeneous photocatalytic hydrogen production from water and biomass derivatives. *Energy Environ. Sci.* **2011**, *4* (7), 2467.

(23) Kang, Y.; Yang, Y.; Yin, L.-C.; Kang, X.; Liu, G.; Cheng, H.-M. An Amorphous Carbon Nitride Photocatalyst with Greatly Extended Visible-Light-Responsive Range for Photocatalytic Hydrogen Generation. *Adv. Mater.* **2015**, *27* (31), 4572−4577.

(24) Yang, S.; Gong, Y.; Zhang, J.; Zhan, L.; Ma, L.; Fang, Z.; Vajtai, R.; Wang, X.; Ajayan, P. M. Exfoliated graphitic carbon nitride nanosheets as efficient catalysts for hydrogen evolution under visible light. *Adv. Mater.* **2013**, *25* (17), 2452−2456.

(25) Liang, Q.; Li, Z.; Huang, Z.-H.; Kang, F.; Yang, Q.-H. Holey Graphitic Carbon Nitride Nanosheets with Carbon Vacancies for Highly Improved Photocatalytic Hydrogen Production. *Adv. Funct. Mater.* **2015**, *25*, 6885−6892.

(26) Nowotny, M. K.; Sheppard, L. R.; Bak, T.; Nowotny, J. Defect Chemistry of Titanium Dioxide. Application of Defect Engineering in Processing of TiO_2-Based Photocatalysts. *J. Phys. Chem. C* **2008**, *112* (14), 5275−5300.

(27) Liu, L.; Chen, X. Titanium dioxide nanomaterials: self-structural modifications. *Chem. Rev.* **2014**, *114* (19), 9890−9918.

(28) Chen, X.; Liu, L.; Yu, P. Y.; Mao, S. S. Increasing solar absorption for photocatalysis with black hydrogenated titanium dioxide nanocrystals. *Science* **2011**, *331* (6018), 746−750.

(29) Niu, P.; Yin, L. C.; Yang, Y. Q.; Liu, G.; Cheng, H. M. Increasing the visible light absorption of graphitic carbon nitride (Melon) photocatalysts by homogeneous self-modifi cation with nitrogen vacancies. *Adv. Mater.* **2014**, *26* (47), 8046−8052.

(30) Kudo, A.; Miseki, Y.; Fujishima, A.; Rao, T. N.; Tryk, D. A.; Fujishima, A.; Zhang, X.; Tryk, D. A.; Fujishima, A.; Honda, K.; et al. Heterogeneous photocatalyst materials for water splitting. *Chem. Soc. Rev.* **2009**, *38* (1), 253−278.

(31) Shen, S.; Shi, J.; Guo, P.; Guo, L. Visible-light-driven photocatalytic water splitting on nanostructured semiconducting materials. *Int. J. Nanotechnol.* **2011**, *8* (6/7), 523.

(32) Li, X.; Hartley, G.; Ward, A. J.; Young, P. A.; Masters, A. F.; Maschmeyer, T. Hydrogenated Defects in Graphitic Carbon Nitride Nanosheets for Improved Photocatalytic Hydrogen Evolution. *J. Phys. Chem. C* **2015**, *119* (27), 14938−14946.

(33) Han, Q.; Wang, B.; Gao, J.; Cheng, Z.; Zhao, Y.; Zhang, Z.; Qu, L. Atomically Thin Mesoporous Nanomesh of Graphitic C_3N_4 for High-Efficiency Photocatalytic Hydrogen Evolution. *ACS Nano* **2016**, *10* (2), 2745−2751.

(34) Fina, F.; Ménard, H.; Irvine, J. T. S. The effect of Pt NPs crystallinity and distribution on the photocatalytic activity of Pt-g-C_3N_4. *Phys. Chem. Chem. Phys.* **2015**, *17* (21), 13929−13936.

(35) Cao, S.; Jiang, J.; Zhu, B.; Yu, J. Shape-dependent photocatalytic hydrogen evolution activity over a Pt nanoparticle coupled g-C_3N_4 photocatalyst. *Phys. Chem. Chem. Phys.* **2016**, *18* (28), 19457−19463.

(36) Xie, Y. P.; Yu, Z. B.; Liu, G.; Ma, X. L.; Cheng, H.-M.; Kudo, A.; Miseki, Y.; Chen, X.; Shen, S.; Guo, L.; et al. CdS−mesoporous ZnS core−shell particles for efficient and stable photocatalytic hydrogen evolution under visible light. *Energy Environ. Sci.* **2014**, *7* (6), 1895.

(37) Cheng, F.; Yan, J.; Zhou, C.; Chen, B.; Li, P.; Chen, Z.; Dong, X. An alkali treating strategy for the colloidization of graphitic carbon nitride and its excellent photocatalytic performance. *J. Colloid Interface Sci.* **2016**, *468*, 103−109.

(38) Li, S.; Dong, G.; Hailili, R.; Yang, L.; Li, Y.; Wang, F.; Zeng, Y.; Wang, C. Effective photocatalytic H_2O_2 production under visible light irradiation at g-C3N4 modulated by carbon vacancies. *Appl. Catal., B* **2016**, *190*, 26−35.

(39) Xiang, Q.; Yu, J.; Jaroniec, M. Preparation and Enhanced Visible-Light Photocatalytic H_2 -Production Activity of Graphene/C_3N_4 Composites. *J. Phys. Chem. C* **2011**, *115* (15), 7355−7363.

(40) Yan, S. C.; Li, Z. S.; Zou, Z. G. Photodegradation performance of g-C_3N_4 fabricated by directly heating melamine. *Langmuir* **2009**, *25* (17), 10397−10401.

(41) Zhu, B.; Xia, P.; Ho, W.; Yu, J. Isoelectric point and adsorption activity of porous g-C_3N_4. *Appl. Surf. Sci.* **2015**, *344*, 188−195.

(42) Zhao, H.; Yu, H.; Quan, X.; Chen, S.; Zhang, Y.; Zhao, H.; Wang, H. Fabrication of atomic single layer graphitic-C3N4 and its high performance of photocatalytic disinfection under visible light irradiation. *Appl. Catal., B* **2014**, *152−153*, 46−50.

(43) Chen, Y.; Wang, B.; Lin, S.; Zhang, Y.; Wang, X. Activation of n → π* Transitions in Two-Dimensional Conjugated Polymers for Visible Light Photocatalysis. *J. Phys. Chem. C* **2014**, *118* (51), 29981−29989.

(44) Li, Y.; Jin, R.; Xing, Y.; Li, J.; Song, S.; Liu, X.; Li, M.; Jin, R. Macroscopic Foam-Like Holey Ultrathin g-C_3N_4 Nanosheets for Drastic Improvement of Visible-Light Photocatalytic Activity. *Adv. Energy Mater.* **2016**, 1601273.